Modified Particle Swarm Optimization With Chaotic Attraction Strategy for Modular Design of Hybrid Powertrains

Quan Zhou, *Member, IEEE*, Yinglong He, Dezong Zhao, Senior *Member, IEEE*, Ji Li, *Member, IEEE*, Yanfei Li, Huw Williams, and Hongming Xu

***Abstract*— This article proposes a new modular design method for hybrid powertrains using a modified accelerated particle swarm optimization (MAPSO) algorithm. The method determines the optimal combination of component specifications and control parameters, where the component specifications include integer variables (e.g., the number of battery modules). A unified chaotic attraction strategy for MAPSO is developed based on a logistic map to improve the probability of achieving the global optimal result. The Pareto analysis is carried out to identify the weighting value for the tradeoff in modular design. The comprehensive reputation score (CRS), considering both Monte Carlo results and the probability of achieving global optima, is employed to evaluate the advantages of the MAPSO compared with conventional PSO and four other PSO variants. The MAPSO is verified as the best because it has the highest CRS. Both two-level and simultaneous methods for modular design are developed with the MAPSO, where the former first operates component sizing at the level 1 and then conducts control optimization at the level 2, and the later optimizes the size and control simultaneously. Compared with the two-level method, the simultaneous method achieves a 7% higher cost function value and saves 50% time.**

***Index Terms*— Chaotic attraction, hybrid vehicle, integer variables, modular design, particle swarm optimization (PSO).**

NOMENCLATURE

P_{fuel}	Equivalent power for fuel consumption.
L_{ice}	Displacement of the engine.
u_{egu}	Engine–generator control command.
vol_{egu}	Dimensional size of the engine–generator.
n_{bm}	Number of battery modules.
R_{eqv}	Battery internal resistance.
I_{batt}	Battery module current.
U_{batt}	Battery module voltage.
r_{cell}	Radius of the battery cell.
h_{cell}	Height of the battery cell.
P_{batt}	Power supplied by the battery pack.
P_{egu}	Power of the engine–generator.
P_{dem}	Vehicle's power demand.
c_{ems}	Control parameters.
$\mathcal{L}$	Set of candidates L_{ice} values.
$\mathcal{N}$	Set of candidates n_{bm} values.
$\mathcal{C}$	Set of candidates c_{ems} values.
p	Population of the particles.
n	Maximum iteration number.
β	Attraction factor.
μ	Tuning parameter in the logistic map.
ER	Error ratio.
GD	Generational distance.

Manuscript received April 20, 2020; revised June 27, 2020; accepted August 3, 2020. Date of publication August 7, 2020; date of current version May 10, 2021. This work was supported in part by the Innovate U.K. under Grant 102253, in part by the EPSRC Fellowship under Grant EP/S001956/1, and in part by the State Key Laboratory of Automotive Safety and Energy, Tsinghua University, under Grant KF2029. *(Corresponding authors: Quan Zhou; Hongming Xu.)*

Quan Zhou and Yanfei Li are with the State Key Laboratory of Automotive Safety and Energy, Tsinghua University, Beijing 100084, China (e-mail: q.zhou@bham.ac.uk).

Yinglong He, Ji Li, Huw Williams, and Hongming Xu are with the Department of Mechanical Engineering, University of Birmingham, Birmingham B15 2TT, U.K. (e-mail: h.m.xu@bham.ac.uk).

Dezong Zhao is with the Department of Aeronautical and Automotive Engineering, Loughborough University, Loughborough LE11 3TU, U.K.

Digital Object Identifier 10.1109/TTE.2020.3014688

I. INTRODUCTION

GROWING concerns for air quality and the advent of zero-emission zones have motivated the automotive industry to seek low-cost carbon emission reduction solutions [1], [2]. The hybridization of vehicles offers a promising solution to energy saving and emissions reduction. Thermal propulsion systems will experience a transition from being the "solo" propulsion device to being part of a "hybrid" system [3]–[5].

Powertrain optimization is critical for the success of hybrid vehicles [6]. Both online and off-line optimization methods are being developed to minimize fuel consumption, emissions, and cost [7], [8]. Model-based predictive control [9], [10], equivalent consumption minimization strategy [11], [12], and reinforcement learning [13]–[15] have been applied to online optimize energy flows of the vehicle. On the other hand, off-line optimization is essential to guarantee the optimal settings of component size and control parameters [16], [17]. It is because changing some key parameters (e.g., engine displacement) is almost impossible once they have been fixed for production.

Modular design allows fast and low-cost development of new vehicular products [18]. Volkswagen develops a modular platform for the flexible development of its new electric and hybrid powertrains [19]. CHANGAN motor unveiled its brandy new "Blue Core" high-efficiency internal combustion

2332-7782 © 2020 IEEE. Personal use is permitted, but republication/redistribution requires IEEE permission.
See https://www.ieee.org/publications/rights/index.html for more information.

Authorized licensed use limited to: UNIVERSITY OF BIRMINGHAM. Downloaded on July 10,2021 at 17:39:41 UTC from IEEE Xplore. Restrictions apply.

engine (ICE) series for hybrid vehicles on a modular platform [20]. Modular design is also widely accepted for the development of off-highway vehicles [21]. Conventionally, the modular design relies on the engineers' experience, while the design results are determined by the design of experiments (DoE) [22]. Artificial intelligence has been deployed for hybrid vehicles for global optimization [16], and this motivates the research into intelligent modular design. The intelligent modular design of hybrid powertrain is an off-line optimization problem on the system level, and there are two typical methods [23], i.e., two-level and simultaneous optimizations.

Two-level optimizations consider component sizing and control optimization as two separated tasks. For component sizing, Pourabdollah *et al.* [24] optimized a hybrid vehicle based on varying levels of modeling details using convex optimization (CO). The optimal component size of a hybrid system considering the cost and battery life has been developed using the Nondominated Sorting Genetic Algorithm (NSGA-II) [25]. Shahverdi *et al.* [26] obtained the Pareto frontier of component cost and fuel economy with a genetic algorithm. Xu *et al.* [27] used the exhaustive search method to optimize the topology of hybrid vehicles considering different powertrain layouts. For control parameters, Wang and Liang [28] optimized the control parameters for energy management to minimize the daily cost using dynamic programming (DP). Lv *et al.* [29] implemented a neural network driver model for control parameter calibration to allow personalized vehicle economy optimization.

Simultaneous optimization deals with the component sizing and control parameter optimization as integrity. Lv *et al.* [30] found the optimal combination of component size and control parameters considering the vehicle dynamic performance, ride comfort, and energy efficiency. Leahey and Bauman [31] optimized the component size and control parameters of a hybrid vehicle using a scripted algorithm. Mamun *et al.* [32] determined the optimal component specification and control parameters of a vehicle using the particle swarm optimization (PSO).

Two-level and simultaneous optimizations have been investigated in many different hybrid vehicle studies, but there is no evidence showing that there exists a universal optimization method for all scenarios [23]. On the other hand, most of the literature assumes that the design variables are continuously varying [33], [34]. The modular design must consider the design variables that are from discontinuously varying domains (e.g., integers). This motivates the development of a modular design method based on the metaheuristic algorithm as it does not require derivation information.

The authors have carried out a series of research on optimization methods for vehicle powertrains with metaheuristic algorithms, including NSGA [35], SPEA [36], [37], and PSO [38], [39]. We chose the PSO variant for the intelligent modular design for the following two reasons: 1) PSO has fewer tuning parameters (compared with NSGA and SPEA) and 2) PSO requires low computational effort (compared with DP) [40] and is flexible for either two-level or simultaneous optimization. The accelerated PSO (APSO) further reduces the number of attraction factors from 2 to 1 and has shown advantages in global searching compared with conventional PSO [41]. Conventional APSO updates the position of its particles with the assumption that the design parameter candidates are continuously varying within their lower and upper boundaries [42]. This article further develops a particle-position-updating strategy to enable optimal searching with mixed-integer variables for modular design.

Chaotic maps have shown the capability of tuning PSO parameters adaptively during the optimization process so that they can improve the convergence speed and the consistency of the optimization results in different trials [43]. Li *et al.* [44] introduced a logistic map to tune the algorithm for gasoline engine optimization. Yu *et al.* [45] implemented a variant of the logistic map (tent map) to tune the PSO parameters for air bearing optimization. The logistic [46], Gauss [47], Singer [48], and sinusoidal maps [49] have been widely studied for parameter tuning in PSO algorithms that deal with continuous-varying variables. However, a unified chaotic attraction strategy for modular design, which deals with mixed-integer variables, has not been reported yet.

To achieve the robustly optimal solution retrieving for the module design of hybrid powertrains, this article proposes a modified APSO (MAPSO) algorithm. This work aims to deliver two new main contributions: 1) the capability of optima searching in discrete-varying domains using the newly proposed MAPSO will be verified, which will resolve the modular design problem with mixed-integer variables and 2) a unified chaotic attraction strategy will be developed based on the logistic map, which tunes the attraction factor of the MAPSO adaptively during the optimization process in modular design. The advantages of the proposed MAPSO will be evaluated compared with the conventional PSO and the APSOs with three commonly used chaotic maps. The evaluation will consider both Monte Carlo results and the probability of achieving global optima. The vehicle performance using the proposed algorithm for both two-level and simultaneous optimizations are demonstrated in both software-in-the-loop and hardware-in-the-loop (HiL) tests.

The rest of this article is organized as follows. Section II provides information about the off-highway vehicle system and the scalable powertrain modules. The optimization problem is formulated in Section III. The APSO algorithm is modified for modular design in Section IV. Experiment platforms are introduced in Section V. The results of experiments are also presented and discussed in Section V. Conclusions are summarized in Section VI.

II. Vehicle and Scalable Powertrain Modules

A. Vehicle System

This article demonstrates the intelligent modular design of a hybrid aircraft-towing tractor, as shown in Fig. 1. The tractor has a series hybrid powertrain using a 245-kW traction motor, which is powered by a battery pack and an engine–generator that provides extra power for vehicle operation and battery charging. The energy management controller determines the amount of power contributed by the engine–generator and the battery package to satisfy the power demand and maintain

Authorized licensed use limited to: UNIVERSITY OF BIRMINGHAM. Downloaded on July 10,2021 at 17:39:41 UTC from IEEE Xplore. Restrictions apply.

Fig. 1. Hybrid aircraft-towing tractor system.

TABLE I
VEHICLE PARAMETERS

Parameter	Description	Value
m_{veh}	Vehicle mass	16t
r_{whl}	Radius of the wheels	0.75m
f_f	Friction coefficient	0.02
C_d	Aerodynamic drag coefficient	0.8
A_f	Effective front area	6.8m^2

the battery state of charge (SoC). Parameters of the vehicle are listed in Table I, and the vehicle is modeled in the Appendix.

B. Scalable Powertrain Modules

Scalable modules, including an engine–generator module, a battery module, and an energy management module, will be optimized in this article to allow a hybrid powertrain achieving its maximum energy efficiency with the minimum geometric size. The engine–generator module and battery module are modeled based on the datasheets provided by the suppliers [37], [50]. The energy management module is developed using a widely used power-distribution function.

1) Engine–Generator Module: The engine–generator module consists of an ICE, a generator, and a fuel tank. The engine model is based on Williams' approximation [25] and assumes a constant bore-to-stroke ratio. The equivalent power of the fuel consumption is scaled by the displacement of the engine

$$P_{\text{fuel}}(t, L_{\text{ice}}) = \frac{L_{\text{ice}}}{L_{\text{ref}}} \cdot H_f \cdot \dot{m}_f(u_{\text{egu}}(t)) \tag{1}$$

where L_{ice} is the displacement of the candidate engine in liters and L_{ref} is the displacement of the baseline engine in liters. In this work, a 4.4-L diesel engine is selected as the baseline. Here, $\dot{m}_f$ is represented by the fuel consumption map, which is based on the engine–generator control command $u_{\text{egu}}(t)$, and H_f is the heat value for the diesel fuel, which is 44×10^6 J/kg.

The dimensional size of the engine–generator vol_{egu} is scaled using a logistic function of the engine displacement L_{ice}

$$\text{vol}_{\text{egu}}(L_{\text{ice}}) = \frac{1}{c_{e1} + e^{-(c_{e2} \cdot L_{\text{ice}} + c_{e3})}} \tag{2}$$

where $c_{e1} = 9.5\text{e} - 5$, $c_{e2} = 0.9006$, and $c_{e3} = 5.685$ are the model parameters, which are calibrated using the MATLAB curve fitting toolbox based on a data set from the supplier [50].

2) Battery Module: Each battery module is assembled by arranging 100 Panasonic 18650 battery cells in series to achieve a nominal voltage of 370 V. A 2-RC battery model is developed and calibrated with the data from [51]. The battery pack is scaled by the total number of the battery module in parallel, n_{bm}. The power loss of the battery is

$$P_{\text{batt\_loss}} = n_{\text{bm}} \cdot R_{\text{eqv}}(t) \cdot I_{\text{batt}}^2(t) \tag{3}$$

where R_{eqv} is the battery internal resistance derived from the battery's SoC. In practice, the battery SoC is observed by the battery voltage $U_{\text{batt}}(t)$ and the current $I_{\text{batt}}(t)$. Therefore, in this article, the battery internal resistance is mapped by the battery voltage and current, i.e., $R_{\text{eqv}}(U_{\text{batt}}(t), I_{\text{batt}}(t))$.

The dimensional volume of the battery package vol_{bp} is scaled by the number of lithium-ion battery cells n_{bc} as

$$\text{vol}_{\text{bp}}(n_{\text{bm}}) = n_{\text{bm}} \cdot 100 \cdot 4 \cdot {r_{\text{cell}}}^2 \cdot h_{\text{cell}} \tag{4}$$

where r_{cell} is the radius of the battery cell and h_{cell} is the height of the battery cell. In this work, r_{cell} and h_{cell} are set as 6.5×10^{-3} and 65.3×10^{-3} m, respectively [51].

3) Energy Management Module: The power supplied by the engine–generator and battery is calculated in real-time by

$$\left.\begin{aligned} P_{\text{egu}} &= u_{\text{egu(SoC)}} \cdot P_{\text{egu\_max}} \\ P_{\text{batt}} &= P_{\text{dem}} - P_{\text{egu}} \end{aligned}\right\} \tag{5}$$

where P_{batt} is the power supplied by the battery pack, P_{egu} is the power supplied by the engine–generator, $P_{\text{egu\_max}}$ is the maximum power that can be provided by the engine–generator, and P_{dem} is the vehicle's power demand.

Energy management strategies, including exponential functions [7], model-based predictive control [9], [10], and model-free control [13], [14], build a nonlinear relationship between the power distribution and the vehicle states (e.g., battery SoC). This article provides a paradigm based on the exponential function because it is robust and provides nonlinear constraints like the other strategies. The engine–generator is, therefore, controlled by [16]

$$u_{\text{egu}}(\text{SoC}) = \begin{cases} 0, & \text{SoC}\epsilon[0.81] \\ e^{\left(-\frac{(\text{SoC}-\text{SoC}^-)^2}{2 \cdot {c_{\text{ems}}}^2}\right)}, & \text{SoC}\epsilon[0.20.8) \\ 1, & \text{SoC}\epsilon[00.2) \end{cases} \tag{6}$$

where c_{ems} is the control parameter to be optimized for power distribution control, SoC is the state of charge of the battery, and SoC^- is the lower battery SoC boundary. Normally, $\text{SoC}^- = 0.2$ is chosen to ensure the battery health.

Authorized licensed use limited to: UNIVERSITY OF BIRMINGHAM. Downloaded on July 10,2021 at 17:39:41 UTC from IEEE Xplore. Restrictions apply.

III. Optimization Problem

The modular design aims to find the optimal combination of components size and energy management parameters. The mathematic model of the modular design is

$$[\,L^*_{\text{ice}}\;\; n^*_{\text{bm}}\;\; c^*_{\text{ems}}\,] = \arg\min\,(\,J_{\text{loss}}\;\; J_{\text{size}}\,) \left\{ \text{s.t.} \begin{cases} L_{\text{ice}} \in \mathcal{L} \\ n_{\text{bm}} \in \mathcal{N} \\ c_{\text{ems}} \in \mathcal{C} \end{cases} \right\} \tag{7}$$

where L^*_{ice} is the optimal engine size, n^*_{bc} is the optimal size of the battery package, c^*_{ems} is the optimal coefficient value for the power distribution function, and $\mathcal{L}$, $\mathcal{N}$, and $\mathcal{C}$ are the value domains of L_{ice}, n_{bm}, and c_{ems}, where $\mathcal{L} = \{2.0, 2.1, 2.2, \ldots, 6.0\}$, $\mathcal{N} = \{55, 56, 57, \ldots, 150\}$, and $\mathcal{C} = \{c_{\text{ems}} \,|\, 0.05 \le c_{\text{ems}} \le 0.2\}$.

The first optimization objective J_{loss} is to minimize the total energy loss over a driving cycle, which can be calculated using the equivalent energy of both fuel consumption and the energy loss in the internal resistance of the battery

$$J_{\text{loss}} = \int_{t_0}^{t_p} P_{\text{fuel}}(t) \cdot dt + \int_{t_0}^{t_p} P_{\text{batt\_loss}}(t) \cdot dt \tag{8}$$

where P_{fule} and $P_{\text{batt\_loss}}$ are calculated by (1) and (3).

The dimensional volume of components is considered in the second optimization objective, which is given by

$$J_{\text{size}} = vol_{\text{egu}}(L_{\text{ice}}) \cdot 10^{-3} + \text{vol}_{\text{bp}} \tag{9}$$

where vol_{egu} is the total volume of engine–generator that is calculated by (2), the volume of engine–generator is multiplied by 10^{-3} to convert the unit from L to m^3, and vol_{bp} is the volume of battery pack calculated by (4).

IV. Modified Accelerated Particle Swarm Optimization Algorithm for Modular Design

This section introduces the idea of the MAPSO algorithm for the modular design of hybrid powertrain for both simultaneous and two-level methods, where the new particle-position-updating strategy and chaotic attraction strategy are newly developed.

A. General Idea

The general idea of the module design with the MAPSO algorithm is using the particle swarm intelligence to retrieve the best position (defined in a Euclidean coordinator compromising the variables needed to be optimized) that achieves the lowest cost in a nonlinear space (defined by the optimization objectives). The simultaneous method optimizes the design parameters and control parameters simultaneously, as shown in Fig. 2(a). The two-level method optimizes the design parameters based on a guess control parameter on the first level and uses the optimized design parameters to find the optimal control parameters on the second level. The optimization results from the two-stage method will be found after several rounds of iteration with different initial guesses of control parameters.

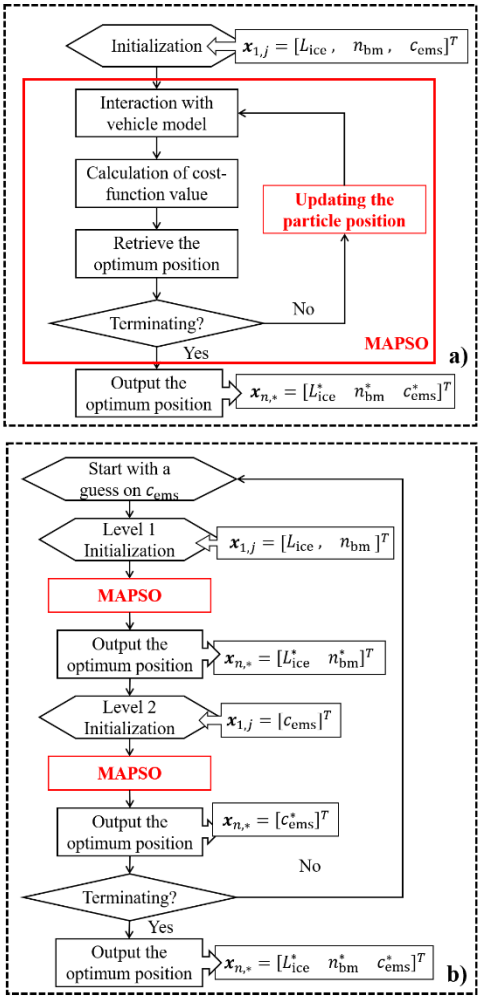

Fig. 2. Flowchart of the modular design with MAPSO. (a) Simultaneous method. (b) Two-level method.

The positions of particles (i.e., computing agents) are defined as following using a Euclidean coordinator:

$$\left.\begin{array}{rl} \boldsymbol{x}_{i,j} = [L_{\text{ice}}, \; n_{\text{bm}}]^{\text{T}}, & \text{lv.1} \\ \boldsymbol{x}_{i,j} = [C_{\text{ems}}]^{\text{T}}, & \text{lv.2} \\ \boldsymbol{x}_{i,j} = [L_{\text{ice}}, \; n_{\text{bm}}, \; C_{\text{ems}}]^{\text{T}} & \text{simultaneously} \\ i = 0, 1, 2, \ldots; \quad j = 1, 2, .., p & \end{array}\right\} \quad \text{two level} \tag{10}$$

where $\boldsymbol{x}_{i,j}$ is the "position" of the jth "particle" at the ith iteration; n is the maximum number of iterations, which is used to terminate the iterations; and p is the population of the particles, which defines the capability of global search in each iteration.

The objective function values are the total power loss $\boldsymbol{J}_{\text{loss}}$ and the total volume of the powertrain components $\boldsymbol{J}_{\text{size}}$, which is obtained by p cases of parallel simulations. A matrix of particle positions $[\boldsymbol{x}_{i,1}, \boldsymbol{x}_{i,2}, \ldots, \boldsymbol{x}_{i,p}]$ is the inputs of the parallel simulation. The simulation is based on the driving cycles that are defined with data from the London Heathrow Airport [17].

Authorized licensed use limited to: UNIVERSITY OF BIRMINGHAM. Downloaded on July 10,2021 at 17:39:41 UTC from IEEE Xplore. Restrictions apply.

B. Particle Positions Update With a Floor Function

Conventional APSO algorithm updates the particle positions by

$$\boldsymbol{x}_{i+1,j} = \boldsymbol{x}_{i,j} + \beta \cdot (\boldsymbol{x}_{i,*} - \boldsymbol{x}_{i,j}) + \alpha^{i+1} \cdot \boldsymbol{r}_{i,j} \tag{11}$$

where $\boldsymbol{r}_{i,j}$ is a vector of unique random numbers for each particle in each iteration, α^{i+1} is a shrinking factor in reducing the influence of random moves, and β is the attraction factor that controls how the global best position will attract the movement of each particle. For the standard APSO algorithm, the value of the attraction factor is fixed, and $\beta = 0.5$ is used [52]. $\boldsymbol{x}_{i,*}$ is the best position in the ith iteration, which is a column of the matrix $[\boldsymbol{x}_{i,1}, \boldsymbol{x}_{i,2}, \ldots, \boldsymbol{x}_{i,p}]$ that satisfies

$$J\left(\boldsymbol{x}_{i,*}\right) \leq J\left(\boldsymbol{x}_{i,j}\right) \tag{12}$$

where $i = 1, 2, \ldots, n$ and $j = 1, 2, .., p$. $J(\boldsymbol{x}_{i,j})$ is the cost function evaluated for each $\boldsymbol{x}_{i,j}$ value, which is calculated with a weighted-sum cost function to integrate the two objectives

$$J(\boldsymbol{x}_{i,j}) = \left(w \cdot \frac{J_{\text{loss}}(\boldsymbol{x}_{i,j})}{J^*_{\text{loss}}} + (1-w) \cdot \frac{J_{\text{size}}(\boldsymbol{x}_{i,j})}{J^*_{\text{size}}} \right) \tag{13}$$

where $\boldsymbol{x}_{i+1,j}$ and $\boldsymbol{x}_{i,j}$ are the position of the jth particles at the $i+1$th and ith iterations, respectively; w is the weighting factor; J^*_{loss} and J^*_{size} are scale factors to ensure that the values of the scaled objective functions are both within 0 and 1; J^*_{loss} is the energy loss determined by using a 6.0L engine–generator to track the tractor's power demand under the combined driving cycle (CDC); and J^*_{size} is the total size of a 6.0-L engine–generator and a battery pack with 150 modules that are calculated by (9).

To deal with the discontinuous variables for component sizing, i.e., for engine–generator $\mathcal{L} = \{2.0, 2.1, 2.2, \ldots, 6.0\}$ and for battery $\mathcal{N} = \{55, 56, 57, \ldots, 150\}$, the proposed MAPSO algorithm modifies (13) as

$$\boldsymbol{x}_{i+1,j} = \frac{\text{floor}[s.(\boldsymbol{x}_{i,j} + \beta \cdot (\boldsymbol{x}_{i,*} - \boldsymbol{x}_{i,j}) + \alpha^{i+1} \cdot \boldsymbol{r}_{i,j})]}{s} \tag{14}$$

where floor(x) is a function that rounds the elements of x to the nearest integers less than or equal to x; s is a scaling factor to generate new position with a resolution; $s = 1$ is for battery module; and $s = 10$ is for engine–generator module because the displacement of the engine is varying with a resolution of 0.1.

C. Chaotic Attraction With Logistic Map

The general idea of chaotic attraction is to develop an iteration-variant attraction factor $\beta(i)$, which generates a set of $\beta \in [0, 1]$ for each iteration, $\{\beta(1), \beta(2), \ldots, \beta(n)\}$, to upgrade the attraction factor in β (13) and (14). The logistic map, which follows a principle of biological evidencing behavior, is proposed as a unified chaotic attraction strategy in this article because it has only one tuning parameter and is easy to be implemented in engineering applications [46]. The logistic map dynamically updates the attraction factor in each iteration as

$$\beta(i) = \mu \cdot \beta(i-1) \cdot (1 - \beta(i-1)) \tag{15}$$

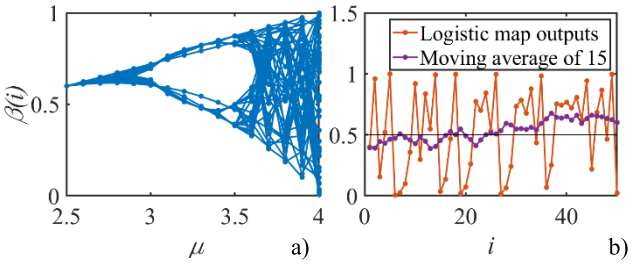

Fig. 3. Chaos behavior of logistic map. (a) Bifurcation diagram. (b) Dynamics in each iteration.

TABLE II
SUMMARY OF DRIVING CYCLE PROFILES

Algorithm	Comb. cycle	RWC-1	RWC-2	RWC-3
Cycle Length	8504s	4907s	4055s	4151s
Mean power demand	39.4kW	32.9 kW	35.5 kW	48.1 kW

where μ is the constant. According to the bifurcation diagram in Fig. 3(a), which illustrates the value of $\{\beta(2), \beta(3), \ldots, \beta(n)\}$ with different settings of μ, $\mu = 4$ is chosen because it covers most values between 0 and 1. The β values in 50 iterations are shown in Fig. 3(b). The average β values (calculated with a moving window compromise 15 samples) are smaller than 0.5 in the first 25 interactions (to have more search around the local area) but are greater than 0.5 after the 25th iteration (to accelerate the convergence). This will theoretically prevent particles from being trapped into local optima in a computationally effective way.

V. Results and Discussion

The experimental study is carried out on both software-in-the-loop (off-line) and HiL (online) testing platforms. The MAPSO algorithm is initially running off-line in MATLAB 2017a on a PC configured with an i7 CPU and 16-GB RAM. Real-world cycles (RWCs) 1–3 are defined using the data collected at the London Heathrow Airport on a tractor working with small, medium, and large airplanes, respectively. The CDC is a random combination of RWC 1–3, which is used for off-line optimization study. The driving cycle profile is illustrated in Table II. Both the CDC and RWC 1–3 are used for the evaluation of the powertrain performance on the HiL platform, as shown in Fig. 4. The performance of the powertrain using the optimized component parameters is emulated in the ETAS LABCAR, controlled by the ES910 with the optimized control parameter.

A. Pareto Frontier for Selection of Weighting Factor

An approximated Pareto Frontier (aPF) for modular design under the CDC, as shown in Fig. 5, is obtained by calculating the nondominated set from the results obtained by the MASPO and the NSGA-II (a benchmark Pareto method) algorithms.

The effectiveness of the estimated PF (ePF) obtained by the MAPSO (with different weighting factors) is validated

Authorized licensed use limited to: UNIVERSITY OF BIRMINGHAM. Downloaded on July 10,2021 at 17:39:41 UTC from IEEE Xplore. Restrictions apply.

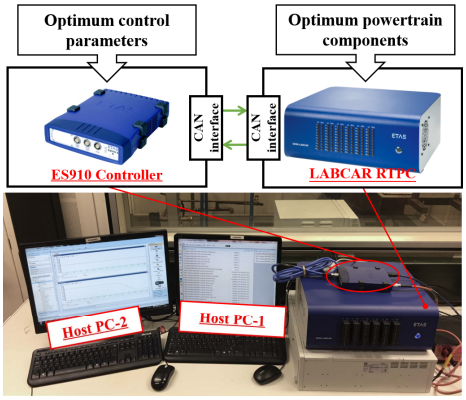

Fig. 4. HiL testing facility.

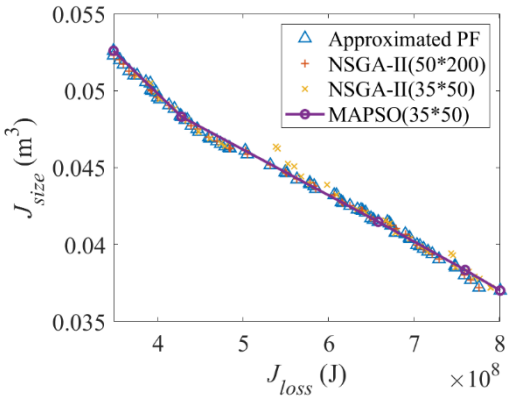

Fig. 5. aPFs in modular design.

by comparing it with the aPF and the ePF obtained by the NSGA-II algorithms with two different settings. A tradeoff analysis based on the ePF will be conducted to guide the selection of the weighting factor of two optimization objectives in MAPSO.

The ePF obtained by the NSGA-II (50*200) algorithm, which has a population size (pop size) of 50 running for 200 iterations, is shown in the red "+" sign. The ePT obtained by the MAPSO, which has a pop size of 35 running for 50 iterations, is shown in purple circles. It illustrates the dominated optimum values of both objective functions (i.e., J_{loss} and J_{size}) with the weighting factor changing from 0 to 1 with a step size of 0.25. The weighting factor of 1 means that the optimization only considers the energy loss, while 0 means that only the minimization of component size is considered. The ePF obtained by the NSGA-II (35∗50), which has the same number of vehicle model iterations as the MAPSO, is shown in the yellow "x" sign. ER and GD are used to evaluate the ePF obtained by the MAPSO and NSGA-II algorithms that are defined by [53]

$$\left.\begin{aligned} \text{ER} &= \frac{\sum_{m=1}^{N} e(y_m)}{N} \\ \text{GD} &= \frac{\sqrt{\sum_{m=1}^{N} y_m.\text{dis}^2(y_m, \boldsymbol{S}_{\text{aPT}})}}{N} \end{aligned}\right\} \tag{16}$$

TABLE III
ER AND GD

Algorithm	MAPSO (35*50)	NSGA-II (35*50)	NSGA-II (50*200)
ER	0.80	0.68	0.94
GD	3.48×10^5	3.89×10^6	9.11×10^4

TABLE IV
STATISTIC RESULTS OF 20 INDIVIDUAL OPTIMIZATION TESTS

Algorithm	J^*	Monte Carlo $\bar{J}$	Monte Carlo σ	$P(J=J^*)$
Con. PSO	0.7375	0.7423	2.05e-6	0.20
Con. APSO	0.7375	0.7405	2.18e-6	0.15
APSO+ Gauss	0.7375	0.7393	2.62e-6	0.35
APSO+ Singer	0.7375	0.7394	2.01e-6	0.25
APSO+ Sin	0.7375	0.7394	3.73e-6	0.20
MAPSO	**0.7375**	**0.7338**	**2.04e-6**	**0.45**

where N is the member of elements in the ePF; y_m is the individual value in the ePF sets; $\boldsymbol{S}_{\text{aPF}}$ is a set that forms the aPF; $e(y_m) = 1$ if $y_m \in \boldsymbol{S}_{\text{aPF}}$; otherwise, $e(y_m) = 0$; and $\text{dis}(y_m, \boldsymbol{S}_{\text{aPF}})$ is the shortest distance between the element y_m and the aPF. The ER and GD of the MAPSO are compared with the NSGA-II methods in Table III.

The ePF obtained by the MAPSO achieves higher ER and lower GD than the one obtained by the NSGA-II with the same number of vehicle model iterations. Although the ePF obtained by the NSGA-II (50*200) is better than MAPSO, it needs 10k vehicle model iterations that require more than five times of the computational effort. As a consequence, the ePF obtained by the MAPSO is shown effective. Based on the ePF obtained by MAPSO, the energy loss can be reduced by 5% through increasing components size by 4% when the weight value changes from 0 to 0.25; and a 42% increase in component size can achieve a 56% energy loss reduction when the weight value changes from 0 to 1. The weighting value of 0.75 is chosen for the rest of the investigation because it saves 46% energy via the sacrifice of a 30% increasing in powertrain size, which has the highest energy-saving/volume-increasing ratio.

B. Comprehensive Reputation Evaluation

By running each of the modular optimization cases under the CDC using conventional PSO, conventional APSO, the proposed MAPSO, and the APSO with three other CAS (i.e., the Gauss map [47], the Singer map [48], and the sinusoidal map [49]) for 20 times independently, statistical results of the cost-function values were obtained and are listed as 0.

All the algorithms can retrieve the same best cost-function value (0.7375), which can be regarded as the global optima. This is achieved by a powertrain using a 2.1-L engine–generator, a battery pack with 82 modules, and a power distribution function coefficient of 0.18. It shows that the

Authorized licensed use limited to: UNIVERSITY OF BIRMINGHAM. Downloaded on July 10,2021 at 17:39:41 UTC from IEEE Xplore. Restrictions apply.

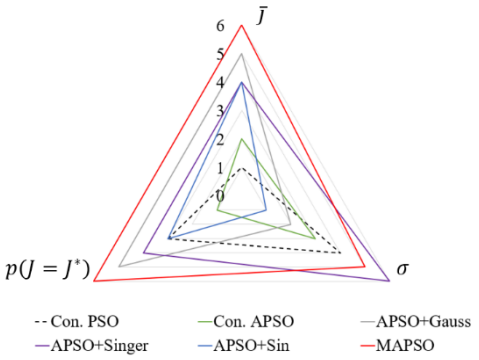

Fig. 6. Scoring of the optimization methods.

modified PSO algorithm can obtain the optimization results with mixed-integer variables. The mean values and standard deviations of the cost-function values obtained by the MAPSO and APSOs with CAS are smaller than the conventional PSO and APSO. MAPSO achieves the minimum mean value (0.7338). APSO with the Singer strategy attains the lowest standard deviation value (2.01e-6) followed by the MAPSO (2.04e-6). The probability of achieving the global best by the MAPSO is 0.45, which is more than twice higher than the conventional PSO ($P(J = J^*) = 0.2$).

The comprehensive reputation scoring system is established based on the ranking of each algorithm in terms of its Monte Carlo results (i.e., mean cost function value $\bar{j}$ and its standard derivation σ) and the probability of achieving global optima $P(J = J^*)$. The higher the ranking the algorithm has, the higher the comprehensive reputation score (CRS) it will gain, e.g., for each evaluation index, the algorithm with the first ranking scores 6, and the sixth ranking algorithm scores 1. The scoring of the six optimization methods is shown in Fig. 6, and the proposed MAPSO is considered as the best for modular design, gaining a CRS of 17, which is more than twice higher than the conventional PSO (CRS = 8).

C. Powertrain Performance With the Optimal Parameters

The powertrain performance using the design parameters obtained by both two-level and simultaneous methods are obtained in Fig. 7. The experiment is carried out in the combined cycle on the HiL platform. The results obtained with the simultaneous method are shown in purple, and the results obtained using two-level methods with initial control parameter guess of 0.05, 0.10, and 0.20 are shown in blue, red, and yellow, respectively.

The results indicate that the hybrid powertrain with the optimized parameters works appropriately: the engine–generator can provide enough power to maintain the battery SoC. In all the given cases, the battery pack can supply enough power, while the voltage and current are within their safe limits. The two-level optimization highly depends on the initial guess on control parameters, and the two-level method with initial $C_{\text{ems}} = 0.20$ achieves the lowest cost-function value of 0.5621, 4.8% better than the two-level optimization with initial $C_{\text{ems}} = 0.05$. The simultaneous method does not need

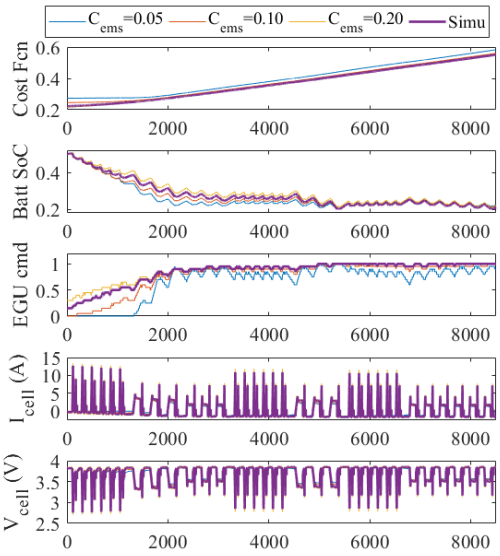

Fig. 7. Powertrain performance in the combined cycle.

TABLE V
VEHICLE ENERGY CONSUMPTION IN DIFFERENT CYCLES

Cycle Name	Method	Cost-fcn value
Combined cycle	Two-level (c=0.05)	0.5905
	Two-level (c=0.1)	0.5813
	Two-level (c=0.2)	0.5621
	Simultaneous	***0.5595***
Real-world cycle 1	Two-level (c=0.05)	0.4043
	Two-level (c=0.1)	0.4016
	Two-level (c=0.2)	0.3982
	Simultaneous	***0.3944***
Real-world cycle 2	Two-level (c=0.05)	0.3799
	Two-level (c=0.1)	0.3760
	Two-level (c=0.2)	0.3717
	Simultaneous	***0.3682***
Real-world cycle 3	Two-level (c=0.05)	0.4250
	Two-level (c=0.1)	0.4137
	Two-level (c=0.2)	0.3981
	Simultaneous	***0.3953***

an initial guess, while it can achieve a cost-function value of 0.5595. In terms of the computational efforts, the average time for the simultaneous optimization in 20 trials is 365.37 s, and it requires 732.27 s for the two-stage method on the same PC. Only three variables are considered for simplification in this work, but the contribution to timesaving is expected to grow exponentially, while the design variables in real practice can be more than hundreds.

D. Robustness of the Modular Design Results

To evaluate the robustness of the optimization results, tests under four different driving cycles are carried out on the HiL platform. The cost-function values affecting the performance of the optimization are listed in Table V. In general, the simultaneous method can achieve better (lower) cost function values compared with the two-stage methods with different initial guesses of the control parameter. Under the combined cycle

Authorized licensed use limited to: UNIVERSITY OF BIRMINGHAM. Downloaded on July 10,2021 at 17:39:41 UTC from IEEE Xplore. Restrictions apply.

(was used for off-line optimization), the cost function value at the end of the HiL test with the results of the simultaneous optimization is 0.5508, which is 5.8% better than that obtained by the two-level method ($c_{\text{ems}} = 0.05$). The reductions of 2.4%, 3.17%, and 7.5% in cost function values have been achieved by the simultaneous method compared with the two-level method ($c_{\text{ems}} = 0.05$) under RWC 1–3, respectively. This indicates that the simultaneous method has a higher potential in cost-function value reduction in the driving cycles with higher average power demand. We can also conclude that the simultaneous method with MAPSO outperforms the two-level methods robustly in the defined driving cycles.

VI. Conclusion

This article proposes a modular design method for hybrid powertrain with a MAPSO algorithm. The probability of achieving the globally optimal result is improved by the chaotic attraction strategy. Experimental studies have been carried out on both software-in-the-loop and HiL platforms. The conclusions drawn from the investigation are as follows.

1) Introducing a weighting value (changing from 0 to 1) in the MAPSO algorithm allows the designer to investigate the sensitivity of the two optimization objectives based on the Pareto frontier. A higher reduction rate in energy loss can be achieved with less increase of powertrain size when the weighting factor is lower than 0.75.
2) Introducing a "floor" function enables the MAPSO algorithms with the capability of optima searching in discrete-varying domains. The proposed MAPSO algorithm has shown robustness in achieving the same best result compared with conventional PSO, conventional APSO, and the APSOs with three other chaos maps.
3) The MAPSO with logistic chaotic attraction strategy is proven as the most effective under the comprehensive reputation scoring scheme. It has the highest CRS of 17, which is at least twice higher than the conventional PSO.
4) MAPSO is compatible with both two-level and simultaneous optimization methods. Compared with the two-level method, the simultaneous method can achieve a 7% better cost function value with 50% less time-consuming.

In the future, the proposed modular design method will be integrated with digital twin models to globally optimize the energy efficiency and safety of connected vehicles.

Appendix

Vehicle Model

The aircraft-towing tractor is modeled backward with the speed profile of driving cycles to calculate the force demand

$$F_{\text{dem}} = F_a + F_d + F_f \tag{A1}$$

where $F_a = (m_{\text{veh}} + m_{\text{plane}}) \cdot (\dot{v}_d/3.6)$, $F_d = (C_d \cdot A_f \cdot v_d^2)/(21.15)$, and $F_f = (m_{\text{veh}} + m_{\text{plane}}) \cdot g \cdot f_f$ are acceleration resistance, air drag, and friction resistance; m_{veh} and m_{plane} are the mass of the tractor and the airplane in kg; v_d is the vehicle speed in km/h; m_{plane} and v_d are defined by driving cycles; C_d and f_f are the drag and rolling resistance coefficient; A_f is the front area of the tractor; and g is the gravity constant. Because the tractor is working on flat grounds, the climbing resistance is ignored. The power and energy demand of the powertrain are calculated by

$$\left.\begin{aligned} P_{\text{dem}} &= \frac{F_{\text{dem}} \cdot v_d}{\eta_{\text{tran}} \cdot \eta_m(n_m, T_m)} \\ E_{\text{dem}} &= \int_{t=t_0}^{t_t} P_{\text{dem}}(t)dt \end{aligned}\right\} \tag{A2}$$

where η_{tran} is the efficiency of the transmission, which is 0.95, according to the datasheet from the supplier; η_m is the efficiency of traction motor, which is a 2-D map of motor speed n_m and torque T_m [17]; and t_0 and t_t are the start time and terminate time in a driving cycle.

References

[1] E. Gregor, "EU legislation in progress CO_2 emission standards for heavy-duty vehicles," Eur. Parliamentary Res. Service, Brussels, Belgium, Tech. Rep., 2019.

[2] *Proposal for Post-2020 CO_2 Targets for Cars and Vans | Climate Action*, Eur. Commission, Brussels, Belgium, 2017.

[3] C. Lv, J. Zhang, Y. Li, and Y. Yuan, "Mechanism analysis and evaluation methodology of regenerative braking contribution to energy efficiency improvement of electrified vehicles," *Energy Convers. Manage.*, vol. 92, pp. 469–482, Mar. 2015.

[4] Q. Zhou, X. Guo, G. Tan, X. Shen, Y. Ye, and Z. Wang, "Parameter analysis on torque stabilization for the eddy current brake: A developed model, simulation, and sensitive analysis," *Math. Problems Eng.*, vol. 2015, pp. 1–10, Jun. 2015.

[5] S. Guo, Z. Chen, X. Guo, Q. Zhou, and J. Zhang, "Vehicle interconnected suspension system based on hydraulic electromagnetic energy harvest: Design, modeling and simulation tests," SAE Tech. Paper 2014-01-2299, 2014.

[6] C. M. Martinez, X. Hu, D. Cao, E. Velenis, B. Gao, and M. Wellers, "Energy management in plug-in hybrid electric vehicles: Recent progress and a connected vehicles perspective," *IEEE Trans. Veh. Technol.*, vol. 66, no. 6, pp. 4534–4549, Jun. 2017.

[7] F. Zhang, X. Hu, R. Langari, and D. Cao, "Energy management strategies of connected HEVs and PHEVs: Recent progress and outlook," *Prog. Energy Combustion Sci.*, vol. 73, pp. 235–256, Jul. 2019.

[8] Y. He *et al.*, "Multiobjective co-optimization of cooperative adaptive cruise control and energy management strategy for PHEVs," *IEEE Trans. Transport. Electrific.*, vol. 6, no. 1, pp. 346–355, Mar. 2020.

[9] Y. Huang, H. Wang, A. Khajepour, H. He, and J. Ji, "Model predictive control power management strategies for HEVs: A review," *J. Power Sources*, vol. 341, pp. 91–106, Feb. 2017.

[10] Q. Zhou, Y. Zhang, Z. Li, J. Li, H. Xu, and O. Olatunbosun, "Cyber-physical energy-saving control for hybrid aircraft-towing tractor based on online swarm intelligent programming," *IEEE Trans. Ind. Informat.*, vol. 14, no. 9, pp. 4149–4158, Sep. 2018.

[11] D. Zhao, R. Stobart, G. Dong, and E. Winward, "Real-time energy management for diesel heavy duty hybrid electric vehicles," *IEEE Trans. Control Syst. Technol.*, vol. 23, no. 3, pp. 829–841, May 2015.

[12] H. Wang, Y. Huang, H. He, C. Lv, W. Liu, and A. Khajepour, "Energy management of hybrid electric vehicles," in *Modeling, Dynamics, and Control of Electrified Vehicles*. Duxford, U.K.: Woodhead Publishing, 2017, pp. 159–206.

[13] T. Liu, X. Hu, S. E. Li, and D. Cao, "Reinforcement learning optimized look-ahead energy management of a parallel hybrid electric vehicle," *IEEE/ASME Trans. Mechatronics*, vol. 22, no. 4, pp. 1497–1507, Aug. 2017.

[14] B. Shuai *et al.*, "Heuristic action execution for energy efficient charge-sustaining control of connected hybrid vehicles with model-free double Q-learning," *Appl. Energy*, vol. 267, Jun. 2020, Art. no. 114900.

[15] Q. Zhou *et al.*, "Multi-step reinforcement learning for model-free predictive energy management of an electrified off-highway vehicle," *Appl. Energy*, vol. 255, pp. 588–601, Dec. 2019.

[16] Y. Huang *et al.*, "A review of power management strategies and component sizing methods for hybrid vehicles," *Renew. Sustain. Energy Rev.*, vol. 96, pp. 132–144, Nov. 2018.

Authorized licensed use limited to: UNIVERSITY OF BIRMINGHAM. Downloaded on July 10,2021 at 17:39:41 UTC from IEEE Xplore. Restrictions apply.

[17] Q. Zhou, W. Zhang, S. Cash, O. Olatunbosun, H. Xu, and G. Lu, "Intelligent sizing of a series hybrid electric power-train system based on chaos-enhanced accelerated particle swarm optimization," *Appl. Energy*, vol. 189, pp. 588–601, Mar. 2017.

[18] B. Schwambach *et al.*, "Conceptualization and implementation of a scalable powertrain, modular energy storage and an alternative cooling system on a student concept vehicle," SAE Tech. Papers 2018-01-1185, Apr. 2018, pp. 1–14.

[19] *The Modular Electric Drive Matrix*, Volkswagen AG, Wolfsburg, Germany, 2019.

[20] *Changan Open New Test Centre and Unveil Blue Core 1.5T Engine*, Changan UK R&D Centre Ltd., Birmingham, U.K., 2019.

[21] *SAE Truck & Off-Highway Engineering: December 2019*, SAE Int., Warrendale, PA, USA, Dec-2019.

[22] A. E. Bayrak, A. X. Collopy, B. I. Epureanu, and P. Y. Papalambros, "A computational concept generation method for a modular vehicle fleet design," in *Proc. 10th Annu. IEEE Syst. Conf. (SysCon)*, Apr. 2016, pp. 1–8.

[23] E. Silvas, T. Hofman, N. Murgovski, L. F. P. Etman, and M. Steinbuch, "Review of optimization strategies for system-level design in hybrid electric vehicles," *IEEE Trans. Veh. Technol.*, vol. 66, no. 1, pp. 57–70, Jan. 2017.

[24] M. Pourabdollah, B. Egardt, N. Murgovski, and A. Grauers, "Convex optimization methods for powertrain sizing of electrified vehicles by using different levels of modeling details," *IEEE Trans. Veh. Technol.*, vol. 67, no. 3, pp. 1881–1893, Mar. 2018.

[25] L. Zhang, X. Hu, Z. Wang, F. Sun, J. Deng, and D. G. Dorrell, "Multiobjective optimal sizing of hybrid energy storage system for electric vehicles," *IEEE Trans. Veh. Technol.*, vol. 67, no. 2, pp. 1027–1035, Feb. 2018.

[26] M. Shahverdi, M. S. Mazzola, Q. Grice, and M. Doude, "Pareto front of energy storage size and series HEV fuel economy using bandwidth-based control strategy," *IEEE Trans. Transport. Electrific.*, vol. 2, no. 1, pp. 36–51, Mar. 2016.

[27] X. Xu, H. Sun, Y. Liu, and P. Dong, "Automatic enumeration of feasible configuration for the dedicated hybrid transmission with multi-degree-of-freedom and multiplanetary gear set," *J. Mech. Des.*, vol. 141, no. 9, pp. 1–14, Sep. 2019.

[28] X. Wang and Q. Liang, "Energy management strategy for plug-in hybrid electric vehicles via bidirectional vehicle-to-grid," *IEEE Syst. J.*, vol. 11, no. 3, pp. 1789–1798, Sep. 2017.

[29] C. Lv *et al.*, "Levenberg–Marquardt backpropagation training of multilayer neural networks for state estimation of a safety-critical cyber-physical system," *IEEE Trans. Ind. Informat.*, vol. 14, no. 8, pp. 3436–3446, Aug. 2018.

[30] C. Lv, X. Hu, A. Sangiovanni-Vincentelli, Y. Li, C. M. Martinez, and D. Cao, "Driving-style-based codesign optimization of an automated electric vehicle: A cyber-physical system approach," *IEEE Trans. Ind. Electron.*, vol. 66, no. 4, pp. 2965–2975, Apr. 2019.

[31] N. Leahey and J. Bauman, "A fast plant-controller optimization process for mild hybrid vehicles," *IEEE Trans. Transport. Electrific.*, vol. 5, no. 2, pp. 444–455, Jun. 2019.

[32] A.-A. Mamun, Z. Liu, D. M. Rizzo, and S. Onori, "An integrated design and control optimization framework for hybrid military vehicle using lithium-ion battery and supercapacitor as energy storage devices," *IEEE Trans. Transport. Electrific.*, vol. 5, no. 1, pp. 239–251, Mar. 2019.

[33] B. Anvari, H. A. Toliyat, and B. Fahimi, "Simultaneous optimization of geometry and firing angles for in-wheel switched reluctance motor drive," *IEEE Trans. Transport. Electrific.*, vol. 4, no. 1, pp. 322–329, Mar. 2018.

[34] M.-J. Kim and H. Peng, "Power management and design optimization of fuel cell/battery hybrid vehicles," *J. Power Sources*, vol. 165, no. 2, pp. 819–832, Mar. 2007.

[35] S. Guo, M. Dooner, J. Wang, H. Xu, and G. Lu, "Adaptive engine optimisation using NSGA-II and MODA based on a sub-structured artificial neural network," in *Proc. 23rd Int. Conf. Automat. Comput. (ICAC)*, Sep. 2017, pp. 1–6.

[36] H. Ma *et al.*, "Model-based multiobjective evolutionary algorithm optimization for HCCI engines," *IEEE Trans. Veh. Technol.*, vol. 64, no. 9, pp. 4326–4331, Sep. 2014.

[37] H. Ma, Z. Li, M. Tayarani, G. Lu, H. Xu, and X. Yao, "Computational intelligence nonmodel-based calibration approach for internal combustion engines," *J. Dyn. Syst., Meas., Control*, vol. 140, no. 4, pp. 1–9, Apr. 2018.

[38] Y. Zhang, Q. Zhou, Z. Li, J. Li, and H. Xu, "Intelligent transient calibration of a dual-loop EGR diesel engine using chaos-enhanced accelerated particle swarm optimization algorithm," *Proc. Inst. Mech. Eng., D, J. Automobile Eng.*, vol. 233, no. 7, pp. 1698–1711, Jun. 2019.

[39] J. Li, Q. Zhou, H. Williams, and H. Xu, "Back-to-back competitive learning mechanism for fuzzy logic based supervisory control system of hybrid electric vehicles," *IEEE Trans. Ind. Electron.*, vol. 67, no. 10, pp. 8900–8909, Oct. 2020.

[40] J. Kennedy and R. Eberhart, "Particle swarm optimization," in *Proc. Int. Conf. Neural Netw. (ICNN)*, vol. 4, 1995, pp. 1942–1948.

[41] X.-S. Yang, "Particle swarm optimization," in *Nature-Inspired Optimization Algorithms*. Amsterdam, The Netherlands: Elsevier, 2014, pp. 99–110.

[42] J. Wan, L. Ding, J. Yao, and H. Wu, "A hybrid CHAOS-PSO algorithm for dimensional synthesis of a redundant manipulator based on tracking trajectories without or with singularities," *Prod. Eng.*, vol. 12, no. 5, pp. 579–587, Oct. 2018.

[43] L.-Y. Chuang, C.-J. Hsiao, and C.-H. Yang, "Chaotic particle swarm optimization for data clustering," *Expert Syst. Appl.*, vol. 38, no. 12, pp. 14555–14563, Nov. 2011.

[44] Z. Li, Q. Zhou, Y. Zhang, J. Li, and H. Xu, "Enhanced intelligent proportional-integral-like fuzzy knowledge-based controller using chaos-enhanced accelerated particle swarm optimization algorithm for transient calibration of air-fuel ratio control system," *Proc. Inst. Mech. Eng., D, J. Automobile Eng.*, vol. 234, no. 1, pp. 39–55, 2019.

[45] Y. Yu, G. Pu, T. Jiang, and K. Jiang, "Discontinuous grooves in thrust air bearings designed with CAPSO algorithm," *Int. J. Mech. Sci.*, vol. 165, Jan. 2020, Art. no. 105197.

[46] A. H. Gandomi, G. J. Yun, X.-S. Yang, and S. Talatahari, "Chaos-enhanced accelerated particle swarm optimization," *Commun. Nonlinear Sci. Numer. Simul.*, vol. 18, no. 2, pp. 327–340, Feb. 2013.

[47] D. He, C. He, L.-G. Jiang, H.-W. Zhu, and G.-R. Hu, "Chaotic characteristics of a one-dimensional iterative map with infinite collapses," *IEEE Trans. Circuits Syst. I, Fundam. Theory Appl.*, vol. 48, no. 7, pp. 900–906, Jul. 2001.

[48] I. Fister, M. Perc, S. M. Kamal, and I. Fister, "A review of chaos-based firefly algorithms: Perspectives and research challenges," *Appl. Math. Comput.*, vol. 252, pp. 155–165, Feb. 2015.

[49] Y. Li, S. Deng, and D. Xiao, "A novel hash algorithm construction based on chaotic neural network," *Neural Comput. Appl.*, vol. 20, no. 1, pp. 133–141, Feb. 2011.

[50] JCB Power Products. (2015). *JCB Generator Technical Specifications*. [Online]. Available: http://www.midas-uk.com/PDF/JCB/QS/G116QS_EN.pdf

[51] Panasonic Automotive & Industrial Systems Europe GmbH. (2017). *Lithium Ion Battery-Cylindrical, Type: UR-18650*. [Online]. Available: https://eu.industrial.panasonic.com/products/batteries-energy-products/secondary-batteries-rechargeable-batteries/lithium-ion-batteries/series/cylindrical-type/ACI4002/model/UR-18650E

[52] B. Chopard and M. Tomassini, "Particle swarm optimization," in *Natural Computing Series*. Amsterdam, The Netherlands: Elsevier, 2018, pp. 97–102.

[53] K. Deb, *Multi-Objective Optimization Using Evolutionary Algorithms*. New York, NY, USA: Wiley, 2001.

Quan Zhou (Member, IEEE) received the Ph.D. degree in mechanical engineering from the University of Birmingham (UoB), Birmingham, U.K., in 2019.

He is currently a Research Fellow with UoB, where he leads the Connected and Autonomous Systems for Electrified Vehicles (CASE-V) Research. His research interests include evolutionary computation, fuzzy logic, reinforcement learning, and their application in vehicular systems.

Dr. Zhou received the UoB's Ratcliffe Prize of the Year. One of his research outcomes has been awarded an Innovate U.K. Grant for commercialization of university research. He received the Visiting Scholar Award from Tsinghua University in 2019 for leading a project that develops digital twin for electrified powertrains. He reviews articles of *Applied Energy* and the IEEE TRANSACTIONS.

Authorized licensed use limited to: UNIVERSITY OF BIRMINGHAM. Downloaded on July 10,2021 at 17:39:41 UTC from IEEE Xplore. Restrictions apply.

Yinglong He received the B.Eng. and M.Res. degrees in energy and power engineering from the Huazhong University of Science and Technology, Wuhan, China, in 2014 and 2017, respectively. He is currently pursuing the Ph.D. degree with the CASE-V Team, University of Birmingham (UoB), Birmingham, U.K.

His research interests include intelligent transportation, vehicle dynamics, driver behaviors, multiobjective optimization, and machine learning.

Dezong Zhao (Senior Member, IEEE) received the B.Eng. and M.S. degrees from Shandong University, Jinan, China, in 2003 and 2006, respectively, and the Ph.D. degree from Tsinghua University, Beijing, China, in 2010, all in control science and engineering.

Since 2017, he has been a Lecturer with the Department of Aeronautical and Automotive Engineering, Loughborough University (LU), Loughborough, U.K. His research interests include connected and autonomous vehicles, machine learning, and control engineering.

Dr. Zhao's work has been recognized by being awarded the EPSRC Fellowship and the Royal Society-Newton Advanced Fellowship in 2018 and 2020, respectively.

Ji Li (Member, IEEE) received the B.S. (Hons.) degree in vehicle engineering from the Chongqing University of Technology, Chongqing, China, in 2015. He is currently pursuing the Ph.D. degree with the CASE-V Team, University of Birmingham (UoB), Birmingham, U.K.

His current research interests include fuzzy mathematics, metaheuristic algorithms, deep reinforcement learning, and man–machine system for intelligent vehicles.

Yanfei Li received the B.Eng. degree in power machinery from Jilin University, Changchun, China, in 2006, and the Ph.D. degree in mechanical engineering from the University of Birmingham, Birmingham, U.K., in 2012.

He is currently a research-focused Assistant Professor with the State Key Laboratory of Automotive Safety and Energy, Tsinghua University, Beijing, China. His research interests include emissions and two-phase flows in the internal combustion engines (ICE), and dedicated ICE design for hybrid vehicles.

Huw Williams received the Mathematics degree from the University of Oxford, Oxford, U.K., in 1978. He is currently pursuing the Ph.D. degree in theoretical mechanics with the University of East Anglia, Norwich, U.K.

He has over 20 years of experience in the automotive industry. He joined Jaguar Land Rover (JLR), Coventry, U.K., in 1986, where he became one of only two people to hold the position of Senior Engineering Specialist in JLR's Product Development Organization. He also developed statistical skills through Total Quality Management (TQM) in the 1980s culminating in his accreditation as Ford's top-scoring Master Black Belt in 2005. He is currently an Honorary Professor with the University of Birmingham (UoB), Birmingham, U.K., and the Director of DEEPPOWER Innovation Ltd. (a university spin-off), London, U.K. He is also a professional mathematician with excellent skills in lean, six sigma, engineering physics, and statistics.

Hongming Xu received the Ph.D. degree in mechanical engineering from Imperial College London, London, U.K., in 1995.

He has six years of industrial experience with Jaguar Land Rover and the Premier Automotive Group, Ford. He is currently a Professor of energy and automotive engineering with the University of Birmingham, Birmingham, U.K., where he is also the Head of the Vehicle and Engine Technology Research Centre. He has authored or coauthored more than 300 journal and conference publications on advanced vehicle powertrain systems involving both experimental and modeling studies.

Prof. Xu was a member of the Ford HCCI Global Steering Committee and the Project Manager and the Technical Leader of the U.K. Foresight Vehicle LINK projects CHARGE and CHASE from 2002 to 2007. He is also a fellow of the SAE International and the Institution of Mechanical Engineers (IMechE).

Authorized licensed use limited to: UNIVERSITY OF BIRMINGHAM. Downloaded on July 10,2021 at 17:39:41 UTC from IEEE Xplore. Restrictions apply.